

Using Branch Predictors to Monitor Brain Activity

Abhishek Bhattacharjee
Department of Computer Science, Rutgers University

ABSTRACT

A key problem with neuroprostheses and brain monitoring interfaces is that they need extreme energy efficiency. One way of lowering energy is to use the low power modes available on the processors embedded in these devices. We present a technique to predict when neuronal activity of interest is likely to occur, so that the processor can run at nominal operating frequency at those times, and be placed in low power modes otherwise. To achieve this, we discover that branch predictors can also predict brain activity. By performing brain surgeries on awake and anesthetized mice, we evaluate several branch predictors and find that perceptron branch predictors can predict cerebellar activity with accuracies as high as 85%. Consequently, we co-opt branch predictors to dictate when to transition between low power and normal operating modes, saving as much as 59% of processor energy.

1. INTRODUCTION

Recent advances in invasive/non-invasive brain monitoring technologies and neuroprostheses have begun shedding light on brain function. Devices such as cochlear and retinal implants, as well as emerging brain-machine interfaces for persons afflicted by spinal cord injuries, motor neuron diseases, and locked-in syndrome are undergoing rapid innovation [1–7]. This is partly because the technologies used to probe and record neuronal activity in vivo are fast improving – we can currently monitor the activity of hundreds of neurons simultaneously, and this number is doubling approximately every seven years [8]. This means that scientists can now study large-scale neuronal dynamics and draw connections between their biology and higher-level cognition.

A natural consequence is that designers are beginning to integrate embedded processors on neuroprostheses to achieve more sophisticated computation than what was previously possible with the simple micro-controllers and analog hardware traditionally used on these devices [1–4, 9–12]. For example, embedded processors are beginning to be used to perform sub-millisecond spike detection and sorting for closed-loop experiments in which a stimulus is immediately delivered to the brain whenever a specific neuron fires [3, 13]. Similarly, brain machine interfaces are replacing bulky and inconvenient wired connections to large desktops with embedded processors [1, 14–16].

These processors face a key obstacle – they need to be energy efficient. Consider the cerebellum, an important portion of the hindbrain of all vertebrates. Recent studies use invasive brain monitoring to record intracellular cerebellar neuronal activity [17–19]. Invasive monitoring implants must typically not exceed stringent 50–300mW power budgets [2, 3, 9–12]. This is because neural implants have small form

factors and must therefore use the limited lifetimes of their small batteries judiciously [2, 3, 9–12]. Equally importantly, stretching out battery lifetimes can reduce how often invasive surgeries for battery replacement and/or recharging are needed. Finally, power consumption must be kept low, as temperature increases in excess of 1-2 degrees celcius can damage brain tissue [20–22]. Unfortunately, the embedded processors used on implants (typically from the ARM Cortex M line) can currently present a barrier to energy efficiency in some systems, expending 35-50% of system energy [2, 3, 23].

A potential solution is to use the low power modes already available on these processors [24–29]. Traditional energy management on server and mobile systems balances the energy savings of low power modes with performance degradation, by anticipating periods of time when applications do not need certain resources or can afford slowdown [24, 27–34]. Similar approaches are potentially applicable to brain implants. Since embedded processors on implants perform signal processing on neuronal spiking data, they could theoretically be placed in low power mode in the absence of neuronal firing and be brought back to nominal operation before neuronal activity of interest. This presents the following problem – how can we predict when future neuronal spiking is likely to occur, both accurately and efficiently?

In response, we observe the following. Architects have historically implemented several performance-critical micro-architectural structures to predict future program behavior. One such structure, the branch predictor, is a natural candidate for neuronal prediction too. Branch predictors assess whether a branch is likely to be taken or not, and as it turns out, map well to the question of whether a neuron fires or not at an instant in time. We study several branch predictors and discover that the perceptron branch predictor [35–39] can accurately predict future cerebellar neuronal activity. We co-opt the perceptron predictor to not only predict program behavior, but to also guide energy management of a cerebellar monitoring implant. Our contributions are:

① We evaluate well-known dynamic hardware branch predictors, including Smith predictors [40,41], gshare [42], two-level adaptive predictors [43], and the perceptron predictor [35]. We perform surgeries on awake and anesthetized mice to extract 26 minutes of neuronal spiking activity from their cerebella and find that perceptron branch predictors are particularly effective at predicting neuronal activity, with accuracies as high as 85%. The success of the perceptron predictor can be attributed to the fact that it captures correlations amongst longer histories of branches better than other approaches. This fits well with cerebellar neuronal activity, where groups of neurons also tend to have correlated activity [17, 19]. These insights set the foundation for future

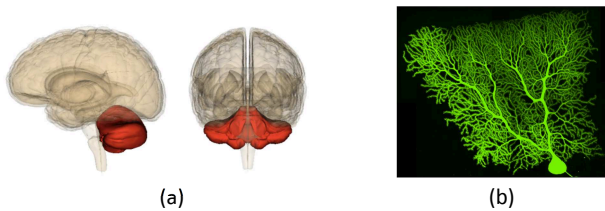


Figure 1: (a) The cerebellum, shown in red, is located behind the top of the brain stem and has two hemispheres [47]; (b) a major cerebellar neuron is the Purkinje neuron, imaged here from a mouse brain [48].

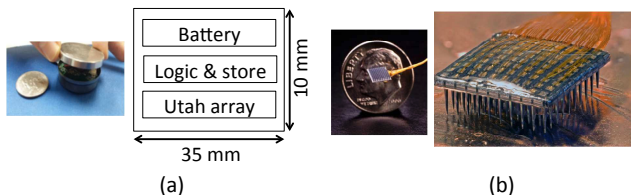


Figure 2: (a) Block diagram of cerebellar implant (dimensions not drawn to scale) and compared against a coin [2]; (b) the Utah array is used to collect intracellular Purkinje recordings [53,54].

studies on using other branch predictors beyond the ones we study [37, 44–46] for neuronal prediction.

② We model a cerebellar monitoring implant. Using architectural, RTL, and circuit modeling, we use the branch predictor to not only predict branches but to also guide energy management. We place the processor in idle low power mode but leave the predictor on to predict brain activity. When the predictor anticipates interesting future cerebellar behavior, it brings the processor back to normal operating mode (where the predictor goes back to being a standard branch predictor). Overall, we save up to 59% of processor energy.

An important theme of this work is to ask – since machine learning techniques inspired by the brain have been distilled into hardware predictors (e.g., like the perceptron branch predictor), can we now close the loop and use such predictors to anticipate brain activity and manage resources on neuroprostheses? Our work is a first step in answering this question. Ultimately, this approach can guide not only management of energy, but also other scarce resources.

2. BACKGROUND

2.1 The Cerebellum

The cerebellum (Latin for “little brain”) affects motor control, language, attention, and regulates fear and pleasure responses [17–19, 49]. It receives input from the sensory systems of the spinal cord and from other parts of the brain, integrating them to fine-tune motor activity. Cerebellar damage leads to movement, equilibrium, and motor learning disorders. Cerebellar damage may also play a role in hallucination and psychosis [50–52]. Figure 1 shows the location of the cerebellum in the human brain and an *in vivo* image of one of its major neuron types, the Purkinje neuron. Our goal is to enable energy-efficient recording of Purkinje activity.

2.2 Cerebellar Monitoring Implants

Figure 2 shows a cerebellar implant, and is typical of recent neural implants [2, 3]. Most neural implants are small and placed in containers embedded via a hole excised in the skull, from where they probe brain tissue. Figure 2 shows that implants typically have the following components:

Microelectrode array: *In vivo* neuronal activity is picked up using microelectrode arrays, which have improved rapidly in recent years [8]. Many implants, including our target system, use Utah arrays made up of several tens of conductive silicon needles that capture intracellular recordings [55–57]. Utah arrays are widely used because of their high signal fidelity, robustness, and relative ease of use.

Logic and storage: Neuronal activity recorded by the Utah array is boosted by analog amplifier arrays connected to analog-to-digital converters (ADCs). While ADC designs vary, 16-channel ADCs produce good signal integrity without excessive energy usage [2, 9]. ADCs route amplified data to memory locations in LPDDR DRAM. Further, flash memory cards are used to store neuronal data [12]. Since GBs of neuronal activity data can be generated in just tens of minutes of recording, most implants use a wireless communication link (typically a GHz RF link) to transmit data to a desktop system with sufficient storage for all the data being recorded. Finally, embedded processors (e.g., energy-efficient ARM Cortex M cores) are integrated on these implants [2, 3, 9, 12]. Our studies focus on an implant with an embedded processor with similar microarchitecture to the Cortex M7 (see Sec. 6 for details). These processors run at 200-300 MHz, but maintain two low-power modes to turn either the processor clock off (to roughly halve processor power consumption) or turn off DRAM and flash too (to lower system power consumption by an order of magnitude) [58].

Battery: Designers commonly use 3.7V batteries to power the implant. Ideally, we want to run implants designed for mice for days or weeks. For primates, we want to push battery lifetimes to months and years. Naturally, the longer the lifetime, the better, since surgeries to replace batteries can be avoided [1]. Wireless charging can reduce the need for surgeries; nevertheless, energy efficiency remains important because neural implants must not raise temperature beyond 1-2 degrees celcius to prevent tissue damage [20–22]. As a result, designers aim to run implants with power budgets of 50-100mW, occasionally permitting higher budgets up to 300mW, if they are for brief periods of time [2, 3, 9, 12].

3. MOTIVATION

Utah arrays and analog components are designed judiciously and turned off when their services are deemed unnecessary [2, 3, 9, 12]. Consequently, today’s embedded processors sometimes use 35-50% of system-wide energy, with components like DRAM, flash, and analog circuits consuming the rest [2]. We attack this bottleneck using low power modes. To do this, we answer several important questions:

What low power modes do we use? We study signal processing workloads that execute whenever there is neuronal activity of interest. Correct operation requires memory and architectural state to be preserved during low power mode. Deep low power modes that lose state are hence infeasible.

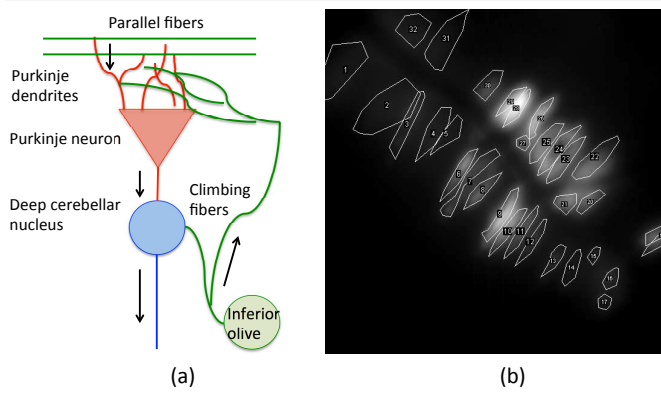


Figure 3: (a) Purkinje neurons are activated by the inferior olive and parallel fibers; and (b) synchronized activity (we surgically collect this image from the cerebellum of a mouse, with Purkinje neurons outlined).

On ARM Cortex processors, with the two low power modes detailed in Sec. 2, this means that we are restricted to using modes that turn off the processor and caches, but not DRAM or flash memory. In the future, as Cortex M7 processors adopt stateful low power modes for DRAM and flash memory [28, 29], we anticipate using them too.

When can we use low power modes? To use low power modes until neuronal activity of interest, we must define the notion of interesting activity. Since neural implants are used for many tasks, this definition can vary. Our study monitors Purkinje neurons in the cerebellum. Purkinje firing therefore constitutes our activity of interest, and can be separated into two classes – unsynchronized and synchronized firing. To understand these firing patterns, consider Figure 3(a), which shows the cellular anatomy of a Purkinje neuron.

Cerebellar Purkinje neurons are driven by two inputs. The first is a set of parallel fibers which relay activity from other parts of the cerebellum. Parallel fibers are connected to Purkinje neurons using the spindly outgrowths of the neurons, i.e., dendrites. The second input is the inferior olivary nucleus, which provides information about sensorimotor stimulation [59]. Inferior olivary nuclei are connected to climbing fibers, which in turn feed Purkinje dendrites.

When either the parallel fibers or the inferior olive fire, spikes are activated on the Purkinje neuron. These spikes drive the deep cerebellar nucleus, influencing motor control and longer-term cerebellar plasticity [17]. The exact nature of Purkinje activity depends on the triggering input. Purkinje spikes due to parallel fibers occur at 17-150 Hz, while those prompted by the inferior olivary nuclei occur at 1-5 Hz [17].

Neuroscientists are studying many aspects of Purkinje spiking, but one that is important is that of synchronized spiking [17, 19, 49, 52]. While single Purkinje neurons usually fire seemingly in isolation, occasionally clusters of Purkinje neurons fire close together in time. Such synchronized firing usually occurs when neighboring olivary nuclei are activated in unison. Figure 3(b) shows imaging data we collect from an anesthetized mouse, where Purkinje neurons have been outlined. The flashing neurons represent firing while those in black represent quiescence. In the time slice shown, several Purkinje neurons fire synchronously.

Given their importance, synchronized firing is our focus.

We enable energy-efficiency by using low power modes when Purkinje synchronization is absent, and using nominal operation when synchronized activity occurs. In so doing, we sustain longer battery life to collect longer and more thorough neuronal recording data for brain mapping studies.

Why do we need neuronal activity prediction? One may initially expect to achieve energy efficiency by placing the processor in sleep mode until the microelectrode array captures synchronized Purkinje activity. At this point, the processor could be transitioned to nominal operating frequency. The problem with this approach is that scientists are curious not just about synchronized activity, but also about milliseconds of individual neuronal activity leading up to synchronized firing [17, 19]. Hence, a better approach is to anticipate synchronized activity sufficiently ahead of time so that events leading up to it are also recorded as often as possible. This necessitates neuronal prediction.

Several prediction strategies initially spring to mind. For example, one could try detecting olivary nuclei activity as an accurate predictor of Purkinje activity. Unfortunately, detecting this activity and separating its effects from those of the parallel fibers requires complex analysis that consumes valuable resources and energy in itself. Alternately, if synchronized firing were to occur with well-defined periodicity, prediction would be simple, but this is not the case [17, 18].

We were intrigued by the prospect of using hardware predictors already on chips today, to also predict neuronal activity. The branch predictor, in particular, springs to mind, as the binary nature of taken/not-taken predictions and outcomes maps naturally to the notion of Purkinje neurons firing or remaining quiet at an instant in time. Furthermore, modern branch predictors can leverage correlations among multiple branches – like correlated branches, the Purkinje neurons that synchronize once often synchronize repeatedly [17]. Purkinje neuron correlations thus fit well with branch predictors, particularly those that capture correlations among long histories of branches, like perceptron branch predictors.

How much energy can we potentially save? To answer this question, we model a baseline with a 300 MHz ARM Cortex M7 processor, and run four workloads often used to process neuronal recordings (see Sec. 6 for details). The workloads read the neuronal data picked up by the Utah array and process it to assess whether it represents synchronized activity. When they identify synchronized activity, they perform additional signal processing on all neuronal activity (synchronized or unsynchronized) in the next 500ms. They then again read neuronal data to assess when the next synchronized event occurs. The baseline does not use the Cortex M7’s idle low power modes because the workloads either continuously profile the neuronal data to detect synchronized activity, or process neuronal spiking during and right after synchronization. Without the ability to predict Purkinje synchronization, the processor cannot know when it is safe to pause execution and use idle low power modes (though in Sec. 7 we do study the potential of using active low power modes like DVFS, if the Cortex M7 were to support them).

We contrast the baseline against an ideal – and hence unrealizable – oracle neuronal activity predictor that knows the future, and imposes no area, performance, or energy over-

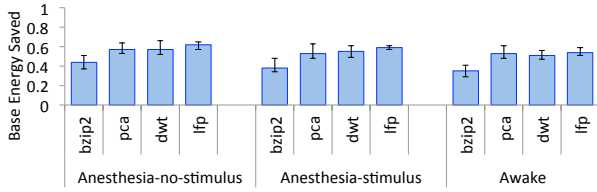


Figure 4: Energy savings due to perfect Purkinje synchronization prediction, assuming that four neurons must fire for synchronization activity. Anesthesia-no-stimulus and Anesthesia-stimulus represent cases where the mouse is under anesthesia with no stimulus and with stimulus respectively, while Awake corresponds to non-anesthetized mice.

heads. This oracle predictor views time in epochs, and is invoked at the end of each epoch to predict whether synchronized Purkinje activity is to occur in the next epoch. Based on the timescales that Purkinje spikes are sustained [17], we assume 10ms epochs. We also consider how many neurons must fire close together in time to be considered synchronized. While scientists may use different counts depending on what exactly they are studying [17], we assume that four firing neurons constitute a synchronized event for now¹. Overall, the processor is suspended in sleep state until the oracle predictor anticipates synchronization. In response, the processor transitions to nominal operation, capturing both the 10ms leadup time to synchronized activity, and the following 500ms of activity. We also model transition times among low power modes. Since these take tens of μ s on Cortex M processors, they have little impact on ms-ranging epochs [60]. Figure 4 quantifies the results for three types of neuronal activity, totaling 26 minutes of Purkinje spiking:

- ① Anesthesia without stimulus: We place mice under deep anesthesia and extract seven 2-minute traces of 32 Purkinje neurons. Anesthetized mice exhibit little movement aside from occasional spontaneous twitching of the limbs, whiskers, and tail. Like past work on synchronized Purkinje firing [17], much of the neuronal activity we study focuses on these experiments since they are the easiest to collect.
- ② Anesthesia with stimulus: To study the effect of controlled sensory stimuli on Purkinje neurons, like past work [17], we apply 20-40 psi air puffs every 40ms to the whiskers of the anesthetized mice. We collect three traces of Purkinje activity, each 2 minutes long. The sensorimotor stimulation from the air puffs increases Purkinje synchronization [17].
- ③ Awake: We collect three 2-minute neuronal traces from an awake free-roaming mouse. The rate of synchronized Purkinje firing varies depending on how the mouse moves.

Figure 4 shows that all benchmarks stand to enjoy significant energy benefits in every single case. We separate energy benefits into average numbers for each of the traces in ①-③, also showing the minimum and maximum values with error bars. With an ideal Purkinje synchronization predictor, energy savings can span 29-65% of total processor energy. Naturally, as Purkinje synchronizations become more frequent (either because mice are stimulated with air puffs or are awake), energy benefits drop since the processor cannot

¹ Sec. 7 shows the impact of varying the number of neurons that must fire to constitute a synchronized event.

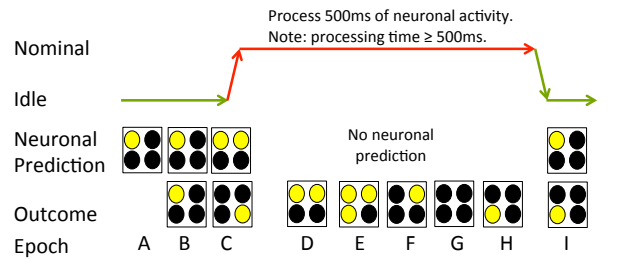


Figure 5: The processor is suspended in idle low power mode, but the branch predictor is kept on to predict Purkinje spiking. When it correctly predicts synchronized Purkinje firing (in this example, two of the four neurons firing), the processor goes to nominal operating frequency.

be placed in sleep mode for quite as long. Still, even in these cases, 63% of energy can be saved with ideal predictors.

4. IMPLEMENTATION

Our goal is to show that branch predictors can be used for neuronal prediction, but there are many potential ways that they could be architected for this purpose. We study a design that uses the same branch predictor to predict branches and neuronal activity as it sufficiently demonstrates the branch predictor’s ability to predict Purkinje activity and guide energy management. However, it may be even better to implement separate branch/neuronal predictors. Our work sets the foundation for future studies of these alternate design points.

4.1 Energy Management Strategies

Figure 5 shows how we manage energy. Since Purkinje activity is usually unsynchronized, the Cortex M7 is placed in idle low power mode, turning off processor and cache clocks but continuing to power DRAM. Our Idle state is different from traditional low power modes in an important way – we keep the branch predictor on, and as described in Sec. 4.2, implement a hardware FSM to use the predictor to predict Purkinje firing instead of branches. Figure 5 shows Neuronal Predictions and actual Outcomes, split into Epochs of time labeled A-I (which are 10ms in our studies). Our example monitors four neurons, shown in circles. Yellow circles represent firing, while black circles represent quiescence; synchronization occurs when at least two neurons fire.

In epoch A, the branch predictor is used for neuronal prediction and anticipates only a single Purkinje neuron firing in the next epoch, B. Consequently, the processor continues in Idle. The prediction is correct as it matches the Outcome in B². Simultaneously in B, the predictor predicts that only one neuron will fire in C. This turns out to be correct again – although the exact neuron that fires does not match the prediction, a concept that we will revisit shortly – and the processor continues in Idle. However, in C, the predictor anticipates a synchronization event between the two top Purkinje neurons. Consequently, the processor is transitioned into Nominal operating mode. Since transition times on the Cortex M7 are orders of magnitude smaller than 10ms epoch times [60], our prediction enables us to awaken the processor sufficiently early to process not only synchronization activity but also

²Sec. 4.2 explains that neuronal activity outcomes are provided by the Utah array and ADCs, which place data in DRAM.

activity leading up to it. Once in nominal operation, the processor analyzes 500ms of Purkinje neuron activity, which can consist of synchronized and unsynchronized spiking, as shown in D-E and F-H respectively. During this time, the branch predictor returns to predicting branches and not neuronal activity. Note that the time taken to analyze 500ms of neuronal activity can exceed 500ms. Finally, the processor again transitions to Idle, with the branch predictor returning to brain activity prediction. Overall, there are four possible combinations of neuronal prediction and outcomes:

- ① **Correctly predicted non-synchronization:** This is desirable to idle the processor as long and often as possible.
- ② **Correctly predicted synchronization:** We want most synchronizations to be correctly predicted, enabling capture of both the activity before synchronization, as well as 500ms of neuronal activity during and after it.
- ③ **Incorrectly predicted non-synchronization:** Occasionally, branch predictors may make mistakes. Figure 6 shows that in epoch C, the branch predictor expects no Purkinje neurons to fire in epoch D. Unfortunately, this prediction turns out to be incorrect, as the top two Purkinje neurons do fire in D. We mitigate the damage caused by this by transitioning to Nominal operating mode as soon as we detect the misprediction. Unfortunately though, the implant still misses the opportunity to monitor pre-synchronization activity. Therefore, we aim to reduce the incidence of this type of misprediction. Note that technically, this kind of misprediction actually saves *more* energy because it runs the processor in Idle for longer (see the blue arrow in Figure 6). However, since it misses important pre-synchronization activity, this type of energy saving is actually undesirable. Overall, we use low power modes to save energy, running the risk that we occasionally mispredict neuronal activity and lose some pre-synchronization activity. But if we reduce the incidence of this type of misprediction, this tradeoff is worthwhile since we ultimately sustain far longer battery life and collect considerably longer neuronal activity recordings overall.
- ④ **Incorrectly predicted synchronization:** Finally, it is also possible for the branch predictor to incorrectly predict synchronized behavior, only to find that this behavior does not occur in the next epoch. This represents wasted energy usage as the processor is transitioned to Nominal operation unnecessarily. However, as soon as we detect no Purkinje synchronization in the following epoch, we transition the processor back to Idle mode.

Recall that in Figure 5, the branch predictor predicted, in B, that the upper left neuron would fire in C. Ultimately the lower right neuron fired. We refer to such predictions as *accidentally correct* as they represent situations where higher-level prediction of synchronization is correct even though the prediction of the individual Purkinje neurons are wrong. Accidentally correct predictions can occur in many ways – for example, the predictor may anticipate a synchronized event with the top two neurons firing, even though the bottom two neurons ultimately fire. While accidentally correct predictions enable correct operation, our goal is to design predictors that are correct in a robust manner, and do not rely on “accidental luck”. We therefore focus on accuracy for both

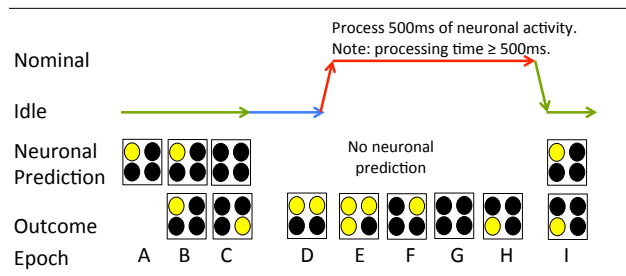


Figure 6: The branch predictor can also mispredict neuronal activity. In this figure, it misses upcoming Purkinje synchronization, so the processor does not record 10ms events leading up to synchronization (in blue), though it is woken up when the misprediction is identified.

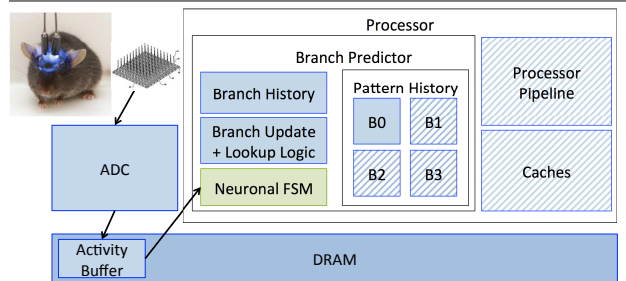


Figure 7: In idle low power mode, striped components are powered off, while a hardware FSM co-opts (part of) the conventional branch predictor for neuronal prediction. Components are not drawn to scale.

per-neuron and synchronized prediction.

Finally, our branch predictor loses state when switching between standard branch prediction and neuronal prediction. This is similar to the impact of context switches [35]. We have found that compared to a baseline that does not use idle low power modes, our approach prompts a 4% drop in branch average prediction accuracy during nominal operation. Since this does not have any discernible performance effect on our implant, and because energy savings are immense (see Sec. 6), we leave more advanced approaches that save branch predictor state for future work.

4.2 Branch/Brain Predictor Implementation

Our modifications leave branch predictor access latencies, energy consumption, etc., *unchanged* in normal operating mode. Therefore, this section focuses on neuronal prediction when the processor is in low power mode. Figure 7 presents the hardware required by our proposal. On the left, we show a mouse with an embedded implant and a Utah microelectrode array used to read out Purkinje activity. This activity is amplified and digitized by the ADC, and stored in a designated DRAM location called an activity buffer.

An important first step in processing the Utah array’s data is to identify which conductive silicon needles on the array correspond to Purkinje neurons. Recall that the Utah array has hundreds of needles. Many of these needles probe non-neuronal tissue, while others probe neurons. Many implants therefore run signal processing code at installation time to associate needles to specific neurons by studying 1-2 seconds of neuronal activity [61]. Since the implant stays in place, once calibration completes, we know exactly which of the Utah array needles correspond to Purkinje neurons. The implant is then free to run its workloads.

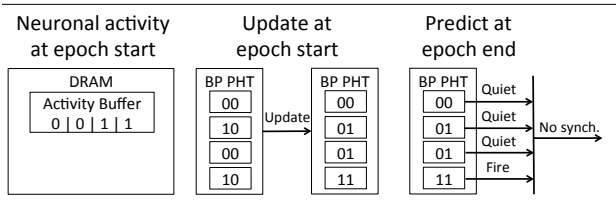


Figure 8: The branch predictor predicts neuronal activity in each epoch in low power mode. We show the Smith predictor as an example.

Figure 7 shows that when these workloads are placed in low power mode, the pipeline and caches are gated off (indicated by stripes). However, the branch predictor is treated differently. We show a general branch predictor structure made up of pattern history tables and branch history tables³. These branch predictor structures are looked up and updated using combinational logic, also shown in the diagram.

When the processor is in idle low power mode, the branch predictor is used to perform neuronal prediction. One option is to leave the entire branch predictor structure on for this purpose. However, this is needlessly wasteful since modern branch predictor tables tend to use tens of KBs with thousands of entries. Meanwhile, modern recording technologies allow us to probe the activity of hundreds of neurons simultaneously [8] so we only technically require hundreds of entries in the branch predictor to make per-Purkinje spike predictions. Therefore, we exploit the fact that modern branch predictors are usually banked [62, 63] and turn off all but one bank. This bank suffices to perform neuronal prediction. To enable this bank to remain on while the remainder of the branch predictor is power gated, we create a separate power domain for it. This requires a separate set of high Vt transistors and control paths. We model the area, timing, and energy impact of these changes (see Sec. 6).

Figure 7 shows that we add a small neuronal FSM (shown in green). We modify the code run in the calibration step after implant installation to add a single store instruction. This updates the contents of a register in the neuronal FSM maintaining a bit-vector used to identify which of the Utah array’s silicon needles probe Purkinje neurons. The neuronal FSM uses this bit vector to decide which entries in the activity buffer store activity from neuronal (rather than non-neuronal) tissue. The neuronal FSM then co-opts the branch predictor for neuronal prediction during idle low power mode. It orchestrates two types of operations, every time epoch:

① Updates with neuronal outcomes: In every epoch, we first update predictor tables with recent Purkinje activity. Consider Figure 8, which shows the DRAM activity buffer at the start of the epoch. The activity buffer maintains an entry for every conductive needle in the Utah array indicating firing (a bit value of 1) and quiescence (a bit value of 0). The neuronal FSM is programmed to know which of these bits correspond to actual neurons via the calibration step. Our example shows entries for four conductive needles probing four neurons, two of which remained quiet and two of which fired at the start of the epoch. Consequently, the neuronal FSM updates the branch predictor bank left on by treating each neuron as a separate branch and updating in a manner

³While our example shows one branch history register, the same approach could be applied to branch history tables too.

that mirrors conventional branch predictor updates. Figure 8 shows this for a Smith branch predictor with 2-bit saturating counters and hysteresis [40, 41]. The four branch predictor entries are used for neurons 0-3, and are updated using the state machine of a standard 2-bit branch predictor.

② Predictor lookups for neuronal predictions: Figure 8 shows that at the end of the epoch, the neuronal FSM must predict whether Purkinje synchronization will occur in the next epoch. Each neuron’s branch predictor entry is looked up to predict whether that neuron will fire. In our example, the first three neurons are predicted to remain quiet while the last one is predicted to fire. Combinational logic assesses whether enough neurons are predicted to fire to constitute synchronization. For our example in Sec. 4.1, where at least two neurons must fire for synchronization, the neuronal FSM assesses that the next epoch will not see synchronization and hence the processor can continue in idle low power mode.

While we do not change access times for branch prediction, we consider timing when the branch predictor is used for neuronal prediction. Using detailed circuit modeling, we have found that since neuronal spiking times (and epoch times) range in the order of milliseconds, the timing constraints of modern branch predictors, which are typically designed for hundreds of MHz and GHz clocks, are easily met.

Finally, an important question is why neuronal prediction is needed in the first place. One may consider sizing the DRAM activity buffer to be sufficiently large to store lead-up activity to synchronization. The processor could be transitioned to nominal operation when synchronization occurs. This approach seemingly preserves lead-up activity to synchronization without needing synchronization prediction. Unfortunately, while this approach suffices for some neuronal implants, it is not a solution for implants which must process neuronal activity as soon as it occurs, rather than deferring to a later time. For example, implants designed to provide stimuli to the brain immediately when a specific neuron fires [3, 13] cannot adopt this approach. Our goal to enable energy management on *all* implant types – therefore, we tackle the harder problem of neuronal prediction.

5. BRANCH AND BRAIN PREDICTORS

5.1 Prediction Strategies

A comprehensive study of all branch predictors is beyond the scope of this paper. Instead, we provide intuition on how their design principles need to be rethought for neuronal prediction. To accomplish this, we focus on:

Smith predictors: These use 2-bit saturating counters with hysteresis (see Figure 8). Each Purkinje neuron is allotted a counter in the prediction table⁴. A branch/neuron’s local history is used to predict future behavior (i.e., correlations among branches/neurons are not exploited). We have found that local history can, to some extent, enable prediction of future activity. But, this approach is too simple to perform accurate neuronal prediction when the mouse roams around and hence sees more complex cerebellar spiking.

⁴Since modern predictors maintain large tables with far more entries than the tens-hundreds of neurons we can currently record, we assume one entry per neuron and no aliasing.

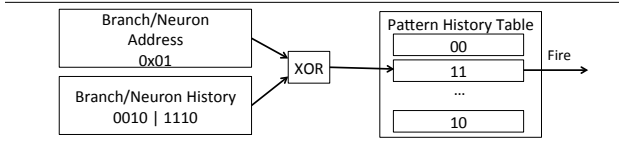


Figure 9: Adapting gshare predictors for neuronal prediction.

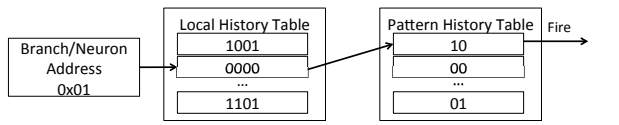


Figure 10: Adapting two-level predictors for neuronal prediction.

Gshare predictors: Smith predictors do not exploit correlations between branches, and hence neurons. This is a problem for Purkinje neurons, which form “micro-bands” or groups where neurons fire close together in time in a synchronized manner [17, 19]. To exploit micro-bands, we study branch predictors that exploit correlated branches. Gshare is a well-known example of such a predictor. Figure 9 shows how gshare predictors can be co-opted for neuronal prediction. The neuronal FSM from Sec. 4 looks up the predictor table for each individual neuron. If enough of them are predicted to fire, a synchronization event is predicted. Figure 9 illustrates lookup for neuron number 1. Gshare performs an exclusive-or between this “address” (or neuron number) and an n -bit global history register, which records the last n branch outcomes globally. For neuronal prediction, one could similarly record spiking behavior of the last n neurons. There are two options – (a) we can record whether there was Purkinje synchronization in the last n epochs (one bit per epoch); or (b) whether each of j individual neurons in the last k epochs (where n equals $j \times k$) fired or not. Recall that our goal is to perform accurate per-neuron predictions, not just synchronization predictions (see Sec. 4.2). We therefore do (b). Figure 9 shows a global history register that stores activity from four neurons in the last two epochs.

Two-level adaptive predictors: It is also possible to exploit inter-branch/neuronal correlations by not just maintaining global history but also per-branch histories. Two-level adaptive predictors leverage this insight [43]. Figure 10 co-opts this approach for neuronal prediction, focusing on the lookup for neuron 1. The neuron number, like the branch address, indexes a table of local history registers. The n -bit registers record outcomes of the last n branches and neuronal data that map to that location. In Figure 10, the local history tables store information on how neuron 1 spiked in the last four epochs (in our example, neuron 1 was quiet in all four epochs). This history selects a saturating counter from the pattern history table, which ultimately determines a prediction for neuron 1 in the next epoch.

Perceptron predictors: Perceptron-based approaches, inspired by machine learning techniques, are best able to leverage inter-branch/neuron correlations. Figure 11 illustrates the operation of a conventional perceptron predictor and how we can adapt it for neuronal prediction [35]. A table of perceptrons – rather than saturating counters – is looked up for each branch or neuron for which we desire prediction. Each perceptron entry maintains weights for each correlated

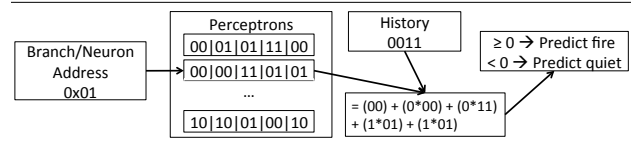


Figure 11: Adapting perceptron predictors for neuronal prediction.

branch/neuron. Like conventional perceptron prediction for branches [35, 36], we use the weights and prior branch outcomes, stored in the history register, to calculate:

$$y = w_0 + \sum_{i=1}^n x_i w_i$$

Here, w_0 is a bias weight, w_i are weights for correlated branches/neurons, x_i are prior branch/neuron outcomes, and y is the output prediction. If y is non-zero, the branch/neuron is predicted taken/fired. In Figure 11, we use 2-bit weights though actual implementations use 8-bit integer weights [35–37]. The weights record a branch/neuron’s dependence on its past behavior through a bias weight, and its dependence on other (four other, in our example) branches/neurons through other weights. All values are stored in one’s complement, like the original design [35], with large positive and negative values indicating positive and negative correlations respectively. Figure 11 shows that the looked-up neuron is weakly correlated with its past (a bias weight of 00) but is positively correlated with neurons 2 and 3 (weights of 01), and strongly but negatively correlated with neuron 1 (weight of 11).

During neuronal prediction, we perform updates in a manner similar to branch prediction [35]. When the neuronal FSM reads the Purkinje spiking outcomes, it checks if there was a misprediction or if the weighted sum’s magnitude was less than a threshold θ (to gauge if training is complete). For either of these situations, the perceptron entry is updated. The algorithm increments the i th weight if the branch/neuron outcome agrees with x_i and decrements it otherwise. We assume the θ values used in prior work for branches [35]; we have found them to suffice for neuronal prediction too.

Because the size of perceptrons scales linearly with the number of correlated branches/neurons, perceptrons exploit longer branch/neuron correlation histories than other schemes, which scale exponentially. This makes perceptron predictions effective at capturing Purkinje micro-bands. Furthermore, the two problems typically associated with perceptron predictors – i.e., high access latency and power consumption [37, 38] – are less of a concern in our design. Access latencies are usually a problem on high-performance GHz-range processors with tight cycle times. Instead, in our system, the processor requires branch predictions on a 300MHz clock or neuronal prediction in 10ms epochs, which perceptron predictors using Wallace tree adders [39] can comfortably achieve. And despite the higher energy requirements of perceptron predictors, their ability to accurately predict neuronal activity enables more aggressive use of low power modes and hence much lower overall system energy.

Figure 11 focused on perceptron prediction using global branch/neuron history. Naturally, it is also possible to perform two-level prediction with perceptrons, where a table of per-branch/neuron histories is first indexed, before looking up the perceptrons. We study this approach too.

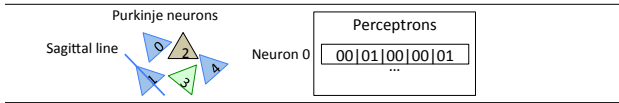


Figure 12: Parasagittal Purkinje neurons spaced a few micron apart are usually correlated. This is reflected in their perceptron table entries.

5.2 Lessons Learned

We summarize key lessons (see Sec. 7 for details).

① **Correlations matter more than local history:** A neuron’s history can provide some indication of future behavior. But local history must be coupled with inter-neuronal correlations for good prediction accuracy. This is because micro-bands of correlated neurons synchronize [17], and predictors that can exploit longer histories of correlated neurons are hence most accurate. Area-equivalent perceptron predictors can achieve 35% prediction accuracy over Smith predictors. Perceptrons also outperform gshare and adaptive predictors.

② **Correlations remain important in the presence of sensorimotor stimulation:** When we blow air puffs on the whiskers of anesthetized mice or study free-roaming mice, Purkinje activity continues to be correlated and synchronization becomes more frequent. Smith predictors, which rely on only local history, drop off in accuracy. For example, awake mice see an average of 27% accuracy, while gshare and two-level adaptive approaches achieve average accuracies of only 35%. Perceptrons continue to exploit inter-neuronal correlations however, and achieve 68% accuracy. We also qualitatively observe that when awake mice move more, perceptron predictors become more accurate than other approaches.

③ **Prediction accuracy trumps higher energy needs:** Two-level adaptive and perceptron approaches consume more power than simpler Smith predictors. We find, however, that complex predictors, especially perceptrons, predict neuronal activity so much more accurately that they can use low power modes aggressively enough to save energy overall.

④ **Neurons experience “phase changes”:** Branch mispredictions often occur when branch correlations change, or when branches are not *linearly separable* for perceptrons. Linear separability refers to the fact that perceptrons can perfectly predict only branches whose Boolean function over variables x_i have its true instances separated from its false instances with a hyperplane, for some values of w_i [39]. Similarly, there are situations when perceptron predictors achieve only 30% neuronal prediction accuracy (and other predictors achieve even less) because many *neurons* are not linearly separable. This is because neurons, just like branches, exhibit phase-like behavior. Groups of Purkinje neurons sometimes switch between micro-bands – i.e., a neuron changes which other neurons it correlates with. This well-known biological phenomenon [17] can lead to mispredictions. We will explore techniques like piecewise linear branch prediction, which target linear separability of branches, [37] to overcome this problem for neurons in the future.

⑤ **Predictors can capture brain physiology:** Parasagittal Purkinje neurons spaced micrometers apart are known to have the highest correlation in behavior [17]. Figure 12 shows that neurons have a sagittal line that divides their bodies into equal left and right sides. Parasagittal neurons are

Pipeline	6-stage, in-order, forwarding
Issue width	2-wide
Instruction and data cache	32KB with ECC
Baseline branch predictor	8KB Smith predictor
Integer/FPU	4-stage/5-stage pipe
Register file	6/4 read/write ports

Table 1: Parameters of our system.

those that are parallel to one another’s sagittal lines. In our example, neurons 0, 1, and 4 are parasagittal and correlated. We have found that perceptron branch predictors accurately capture correlations among parasagittal Purkinje neurons, maintaining much larger weights for them. We have found that on average, the weights for parasagittal neurons are 50%+ larger than the weights for other neurons. Figure 12 shows an example where the weights for neuron 1 and 4 show positive correlation in neuron 0’s perceptron entry.

6. METHODOLOGY

Simulation infrastructure: We model a processor similar to the ARM Cortex M7, with the configuration of Table 1. This paper performs early-stage design exploration. Therefore, rather than implement the chip in hardware, we rely on careful cycle-accurate software simulation. Our processor runs at 300MHz and maintains the standard Cortex M7 idle low power mode where pipelines and caches can be gated off to save power. We use CACTI [64] and McPAT [65] for power/energy analysis. We model the area, timing, and energy implications of creating a separate power domain for the branch predictor bank for neuronal prediction. The additional Vt transistors and control wiring/logic increases chip area by 1.4%. Branch prediction access latencies remain unchanged, however. Further, we model the addition of the neuronal FSM as part of our analysis. In general, we find that its simplicity means that it can be implemented with area-efficient and energy-efficient combinational logic.

Workloads: We use four neuronal spiking analysis workloads, selected for their common use in the neuroscience community, to extract biologically relevant data from neuronal recordings [61]. The four workloads are:

- ① **Compression:** We use **bzip2** to compress the spiking data recorded by the ADC for 500ms after synchronization.
- ② **Artifact removal:** Microelectrode arrays can often pick up noise caused by muscle movement in the scalp, jaws, neck, body, etc. These artifacts can be removed with principal component analysis. Our **pca** benchmark stacks the data from our electrodes, and for each electrode, projects into the PCA domain, yielding cleaned signals [61].
- ③ **LFP extraction:** In **lfp**, we apply a fifth-order Butterworth filter on the neuronal data to enhance low-frequency signals in the range of 0.5-300Hz, as is common practice [61].
- ④ **Denosing:** Reducing noise in neuronal recordings is an important step in neuronal processing. There are several ways to denoise, but we use discrete wavelet transforms or **dwt** with Rigrsure thresholding, similar to prior work [61].

Mouse surgeries: To perform early design space exploration, we extract neuronal activity from mice in vivo, before actually designing the implant. We rely on the emerging field

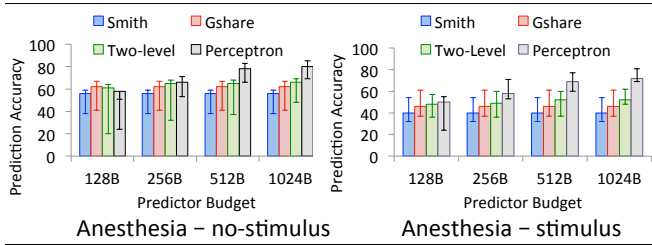


Figure 13: Prediction accuracies for mice under anesthesia without stimulus, and with air puffs blown into their whisker pads. Prediction accuracies are shown as a function of the hardware budget available for the bank of the branch predictor left open.

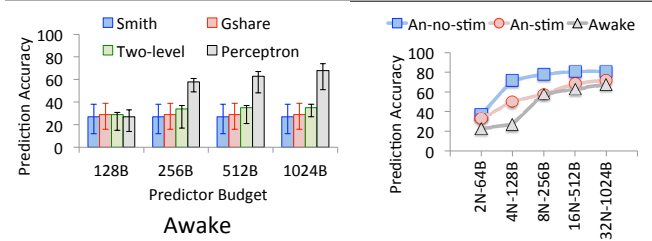


Figure 14: (Left) Prediction accuracy for awake free-roaming mice, as a function of the predictor area budget; and (right) perceptron predictor accuracy as a function of the neuron history length.

of optogenetics for this. Optogenetics gives neuroscientists the ability to use pulses of light to image and control almost any type of neuron in any area of the brain, with precise timing. We perform surgeries on C57BL/6 mice on postnatal days 21-42. We perform small craniotomies of approximately 2mm diameter over lobule 6 locations on the mice cerebella, from which we collect Purkinje activity. For mice under anesthesia, we use ketamine/xylazine to achieve deep anesthetized state. Further, we load the Purkinje cells of the area of study with calcium indicator Oregon Green BAPTA-1/AM (Invitrogen), as described previously [19]. This indicator fluoresces under exposure to light, allowing us to collect images such as Figure 3 using two-photon microscopes [17]. We track the activity of 32 Purkinje neurons.

7. RESULTS

Predictor organizations (i.e., pattern history table and branch history register dimensions, etc.) that maximize neuronal prediction may be different from those that optimize traditional branch prediction. But since branch prediction has been studied for decades, our focus is on neuronal prediction in this paper. We will study the best “compromise” branch/neuronal predictor organizations in future work.

Per-neuron prediction accuracy: We first quantify prediction accuracy for individual Purkinje neurons. We study the cross product of recordings on awake and anesthetized mice (with and without air puffs) and our four benchmarks. This represents 13×4 or 52 experiments. We separate results for Awake and anesthetized mice with air puffs (Anesthesia-stimulus) and without (Anesthesia-no-stimulus).

Figure 13 presents results for anesthetized mice. The y-axis plots per-neuron prediction accuracy, with higher numbers being better. The x-axis shows the hardware budget for the predictor (one branch predictor bank) from 128 bytes to

1KB. Modern branch predictors are 8-16KB, and even 1KB represents reasonable size estimates for bank (which is all we need for neuronal prediction). For each hardware budget, we have exhaustively studied predictor organizations and report results from the organization with the best average accuracy. At each hardware budget, we find that gshare and two-level predictors perform best when they maintain history for $0.5-0.6 \times$ the neurons as the perceptron.

Figure 13 shows that perceptrons predict Purkinje neuron activity more accurately than other approaches, particularly with larger budgets. Smith predictor accuracies remain flat since even the smallest size (128 bytes) has enough area to maintain per-neuron counters. Therefore, when hardware budgets increase to 512 bytes or 1KB, Smith predictors cannot exploit the additional area, while perceptron predictors can. At larger areas, predictors that exploit inter-neuron/branch correlation like gshare and two-level adaptive schemes perform much better. At modest hardware budgets of 1KB, perceptron predictors achieve average prediction accuracy of 80%, and as high as 85%. Perceptrons become even more accurate compared to other approaches when sensorimotor stimulation – and hence the complexity of Purkinje activity – increases (see Anesthesia-stimulus results). While blowing air puffs into whiskers does make it difficult to predict neuronal behavior, perceptron branch predictors still achieve accuracies of 72% for 1KB hardware budgets.

The left side of Figure 14 shows results for awake mice. The increased complexity of neuronal spiking prompts Smith, gshare, and two-level adaptive predictors to mispredict more often. The two-level adaptive scheme only achieves 35% accuracy. However, perceptrons still achieve an average of 68%. Qualitatively, we found that prediction accuracy varies more dramatically when the mouse moves not only its tail but also its limbs (see the larger min/max bars).

The graph on the right of Figure 14 shows how perceptrons achieve more accuracy. We show accuracy as we vary the number of weights stored in each perceptron entry. A label of $jN-kB$ on the x-axis indicates j potentially correlated neurons, totaling k bytes (assuming that we need a separate perceptron entry for every neuron we want to predict). The larger k is, the greater the correlation history amongst branches/neurons, and the more accurate our neuronal prediction. When we plotted this data, we noticed an interesting relationship between the number of weights required for accurate predictions and the biology of Purkinje neurons. Studies have shown that usually a handful (2 to 8) of neurons form micro-bands [17]. The graph on the right of Figure 14 mirrors this observation, with sharp accuracy benefits when the number of weights in the perceptron goes from 2 to 8, particularly when the mouse is awake.

Synchronization prediction accuracy: So far, we have discussed prediction accuracy for each individual Purkinje neuron’s behavior. However, our aim is to ultimately predict synchronization behavior. We focus on the perceptron predictor for these studies as they are far more accurate than other approaches. While good prediction accuracy for individual neurons is a good indicator of synchronization prediction, their relationship is complicated by two competing factors. On the one hand, accidentally correct predictions may occur (see Sec. 4.1), boosting synchronization prediction

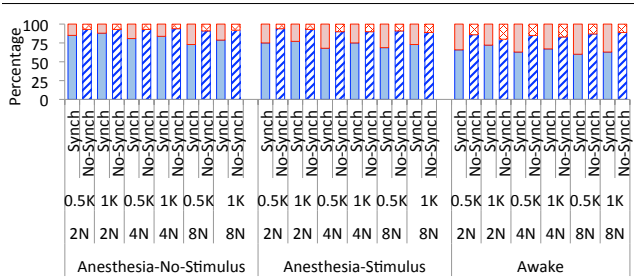


Figure 15: Percentage of synchronized events predicted correctly (solid blue) and incorrectly (solid red), and percentage of unsynchronized events predicted correctly (striped blue) and incorrectly (striped red). We show average results as we vary the number of neurons in a synchronized event from 2, 4, to 8, and as the predictor size varies between 512 bytes and 1KB. All results are for perceptron predictors.

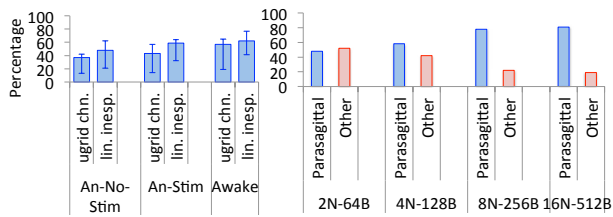


Figure 16: (Left) Percentage of Purkinje neurons that experience micro-grid changes (ugrid-chn.) and are linearly inseparable (lin. inesp.) with averages, min/max shown; and (right) for each neuron predicted to fire, percentage of total weighted sum value contributed by the weights from parasagittal neurons versus others.

accuracy. On the other hand, synchronization requires *multiple* neurons to be simultaneously predicted correctly. The probability that multiple neurons are concurrently predicted accurately is lower than accuracy for an individual neuron.

Figure 15 summarizes synchronization prediction accuracy. We separate results for awake and anesthetized mice, varying the perceptron predictor hardware budget between 512 bytes (0.5KB) and 1KB. We vary the number of neurons that must simultaneously fire to be considered a synchronized event from 2 to 8 (represented by 2N, 4N, and 8N). For each of these cases, we plot two bars. The first bar stacks the percentage of total synchronized events that are correctly predicted (solid blue) and incorrectly predicted (solid red). The second bar stacks the percentage of total non-synchronized events that are correctly predicted (striped blue) and incorrectly predicted (striped red). For both bars, we desire higher contributions from the blue stacks.

Figure 15 shows that perceptrons accurately predict most synchronized and non-synchronized events. Accuracy increases with larger predictors, but remains consistently 75%+ under anesthesia with no stimulus. Naturally, stimuli and awake states make prediction harder, but perceptrons still consistently predict correctly more than 60% of the time.

Figure 15 also shows that prediction accuracies diminish as the number of neurons for a synchronized event increases from 2 to 8. This is expected; the higher the threshold for synchronization, the more the number individual neurons that have to be predicted correctly. Despite this, prediction accuracies decrease by only 10% at worst.

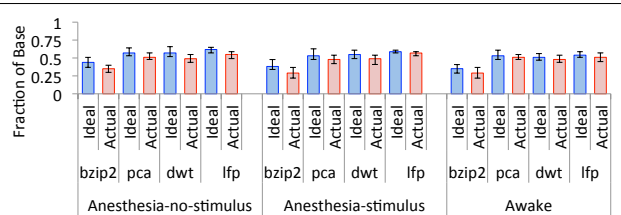


Figure 17: Fraction of baseline energy saved using Ideal and Actual prediction. We assume perceptrons with 32 8-bit weights (1KB budget) and that 4 neurons must fire to be considered synchronized.

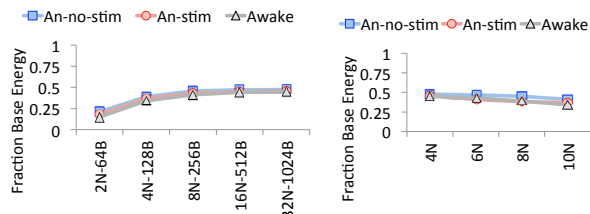


Figure 18: (Left) Average fraction of baseline energy saved when using a perceptron predictor, for different numbers of weights. We assume that 4 neurons must fire to be considered synchronized; and (right) average energy saved when using a perceptron predictor with 32 8-bit weights (1KB total budget) and varying the number of neurons that must fire to be considered synchronized from 2 to 10.

Understanding prediction characteristics: We now discuss the source of mispredictions, focusing on perceptrons as they predict neuronal behavior most accurately. Like branch misprediction, most neuronal misprediction arises from neurons that are linearly inseparable. Past work identifies the fraction of static branches that are linearly inseparable to understand mispredictions [35]. The graph on the left in Figure 16 does the same, but for neuronal prediction (lin. inesp.). There is a biological basis for linear inseparability – neurons sometimes change which other neurons they correlate with. We study our neuronal traces and every 10ms, identify micro-grids. As a fraction these samples, we plot the percentage of time that neurons change between micro-grids (ugrid chn). Figure 16 shows that adding sensorimotor stimulation (An-Stim and Awake) increases micro-grid switches and linearly inseparable neurons, lowering prediction accuracy.

The graph on the right in Figure 16 shows that perceptron predictors also accurately capture the biology of parasagittal correlations. Every time the predictor predicts firing activity, we log what percentage of the perceptron’s weighted sum originates from weights of parasagittal neurons. The higher the percentage, the higher the correlations between parasagittal neurons. We plot these percentages in blue (with the rest shown in red), as a function of the perceptron predictor size and number of weights in each perceptron entry (e.g., jN-kB indicates j weights and k bytes). As expected, with more weights, parasagittal correlations are more easily tracked.

Global versus global/local perceptron histories: Beyond perceptrons with global history, we have also studied a mix of local and global history [39]. Because prediction accuracy hinges on neuronal correlations, we see little benefit (less than 1% more accuracy) from the addition of local history.

Energy savings of perceptrons: Figure 17 quantifies the fraction of energy saved versus the baseline without neuronal prediction described in Sec. 3. The baseline uses an 8KB Smith branch predictor, which we replace with other branch predictors. Though we subsequently revisit the energy benefits of using Smith, gshare, and two-level adaptive predictors for neuronal prediction, we focus on perceptron predictors for now as their energy benefits far outweigh the other approaches. Figure 17 assumes 1KB perceptron predictors, and that four neurons must fire close together in time to be considered a synchronized event.

Figure 17 shows that our energy savings (Actual) achieve within 5-10% of the Ideal energy savings from oracular neuronal prediction. Overall, this corresponds to energy savings of 22-59%. Naturally, applying stimuli to the mouse generally decreases energy saving potential since there are more synchronized events. Nevertheless, the neural implant still achieves 22-50% energy savings on Awake mice.

Figure 18 sheds more light on energy trends. The graph on the left shows the energy saved as the number of 8-bit weights per perceptron entry varies from 2 to 32. More weights improve predictor accuracy by capturing micro-grid correlations. Increasing the number of weights from 2 to 8 doubles energy savings for anesthetized and awake mice. Meanwhile, the graph on the right shows the average energy saved by a 1KB perceptron predictor (with 32 weights per entry), as we vary the number of neurons that must concurrently fire to be considered a synchronized event. As the number of neurons increases, energy savings decrease as there are fewer instances of synchronized events. Nevertheless, even when we assume that 10 neurons must fire to constitute synchronization, we save an average of 30%+ of energy. And since scientists generally study micro-grids of 4-8 neurons [17], average energy savings are closer to 45%+.

Undesirable energy savings: In Sec. 4.1, we illustrated situations where the branch predictor predicts no synchronization, only to find that it does occur. This loses important pre-synchronized activity, so its energy savings are undesirable. We have quantified the percentage of energy savings that are undesirable – they are less than 2% of total energy savings for all workloads. The reason this number is small is that perceptrons have good prediction accuracy. The (few) mispredictions idle the processor for an extra 10ms (the time taken to identify the misprediction). Subsequently, the processor transitions to nominal operation. Compared to the long stretches of times that the processor is correctly predicted and placed in idle low power mode (10s of seconds), these mispredictions minimally affect energy saved.

Energy savings versus other branch predictors: We have focused on perceptron predictors since they consistently save more energy than other approaches. Smith, gshare, and two-level adaptive predictors are simpler and enjoy lower access energies, but their lower prediction rates means that they save, on average, 5-45% less energy than perceptrons.

Impact of branch prediction on program behavior: Of course, the choice of branch predictor also impacts the runtime of the four workloads in Sec. 6. While sophisticated predictors can consume higher access energy, they may also save overall energy if they cut down runtime sufficiently. We

have found that while perceptron branch predictors do increase energy usage when the processor is in nominal operating mode (compared to Smith and gshare prediction), they still save considerably more energy overall because the potential energy savings from neuronal prediction far outweigh any energy impact of performing branch prediction.

Energy savings with dynamic voltage/frequency scaling: We have focused on idle rather than active low power modes like dynamic voltage/frequency scaling (DVFS). This is because Cortex M processors currently support only the former. However, we were curious about energy savings if DVFS were to be incorporated. Therefore, we studied and compared three schemes using a 1KB perceptron predictor: (1) use idle low power modes as described thus far; (2) use DVFS instead of neuronal prediction, to identify opportunities when the workloads can afford to be slowed down to $0.5\times$ and $0.75\times$ of the baseline frequency using standard CPU utilization based prior approaches [28]; and (3) combine (1) and (2) by showing that DVFS and idle mode usage with neuronal prediction are orthogonal. We found that (2) remains superior to (1), saving an average of 12% more energy. Combining neuronal prediction and idle low power modes with DVFS promises even more energy savings (as high as 67%, exceeding the 59% of neuronal prediction alone).

8. CONCLUDING REMARKS

Generality of observations: How conclusively can we say that branch predictors, or indeed any hardware predictors, can predict brain activity? To answer this question, we need to study much more than just 26 minutes of neuronal activity, from more locations than just lobule 6 of the cerebellum. Our study is but a first step in this direction.

Alternate predictors: Perceptron predictors cannot accurately predict brain activity in some cases. A promising direction may be to study hardware that implements richer machine learning techniques to predict dynamic program behavior, like reuse distances of cache lines [66]. Perhaps it may even be possible to co-opt more sophisticated hardware neural networks currently being studied [67, 68], or rely on intelligent software machine learning techniques.

Modeling brain circuits: Neuroscientists are activity seeking to model neural circuits that explain neuronal biology [69]. It may be fruitful to consider whether models of well-known microarchitectural structures like branch predictors could aid neural circuit modeling, particularly if the microarchitectural structures predict neuronal activity accurately.

Related work: Our work is related to hardware neural network accelerators [67, 68, 70–74], but is closer to studies that link neural biology with computer architecture. For example, Hashmi et. al. studied fault tolerance in cortical microarchitectures [75] while Nere et. al. emulated biological neurons digitally [76]. Their work paved the way for Smith’s pioneering studies on efficient digital neurons for large-scale cortical architectures [77]. We are inspired by these studies but focus on co-opting *existing* microarchitectural structures to predict neuronal activity and manage power/energy.

9. REFERENCES

- [1] B. Graimann, B. Allison, and G. Pfurtscheller, "Brain-Computer Interfaces: A Gentle Introduction," *The Frontiers Collection*, 2010.
- [2] Y. Su, S. Routhu, K. Moon, S. Lee, W. Youm, and Y. Ozturk, "A Wireless 32-Channel Implantable Bidirectional Brain Machine Interface," *Sensors*, vol. 16, no. 1582, 2016.
- [3] S. Zanos, A. Richardson, L. Shupe, F. Miles, and E. Fetz, "The Neurochip-2: An Autonomous Head-Fixed Computer for Recording and Stimulating in Freely Behaving Monkeys," *IEEE Transactions on Neural Systems and Rehabilitation Engineering*, vol. 19, no. 4, 2011.
- [4] X. Liu, B. Subei, M. Zhang, A. Richardson, T. Lucas, and J. V. der Spiegel, "The PennBMBI: A General Purpose Wireless Brain-Machine-Brain Interface System for Unrestrained Animals," *IEEE International Symposium on Circuits and Systems*, 2014.
- [5] C. Muhl, B. Allison, A. Nijholt, and G. Chanel, "A Survey of Affective Brain Computer Interfaces: Principles, State-of-the-Art, and Challenges," *Brain-Computer Interfaces*, vol. 1, no. 2, 2014.
- [6] A. S. Ferreira, L. C. de Miranda, E. C. de Miranda, and S. G. Sakamoto, "A Survey of Interactive Systems Based on Brain-Computer Interfaces," *SBC Journal on 3D Interactive Systems*, vol. 4, no. 1, 2013.
- [7] G. Mone, "Sensors on the Brain," *Communications of the ACM*, vol. 60, no. 4, 2015.
- [8] I. Stevenson and K. Kording, "How Advances in Neural Recording Affect Data Analysis," *Nature Neuroscience*, vol. 14, 2011.
- [9] G. N. Angotzi, F. Boi, S. Zordan, A. Bonfanti, and A. Vato, "A Programmable Closed-Loop Recording and Stimulating Wireless System for Behaving Small Laboratory Animals," *Scientific Reports*, vol. 4, no. 5963, 2014.
- [10] T. Nguyen, Z. Navratilova, H. Cabral, L. Wang, G. Gielen, F. Battaglia, and C. Bartic, "Closed-Loop Optical Neural Stimulation Based on a 32-Channel Low-Noise Recording System with Online Spike Sorting," *Journal of Neural Engineering*, vol. 11, no. 4, 2014.
- [11] M. Hirata, K. Matsushita, T. Suzuki, T. Yoshida, F. Sato, S. Morris, T. Yanagisawa, T. Goto, M. Kawato, and T. Yoshimine, "A Fully-Implantable Wireless System for Human Brain-Machine Interfaces Using Brain Surface Electrodes: W-HERBS," *IEEE Transactions on Communications*, vol. E94-B, no. 9, 2014.
- [12] C. Mestais, G. Charvet, F. Sauter-Starace, M. Foerster, D. Ratel, and A. L. Bernabid, "WIMAGINE: Wireless 64-Channel ECoG Recording Implant for Long Term Clinical Applications," *IEEE Transactions on Neural Systems and Rehabilitation Engineering*, vol. 23, no. 1, 2014.
- [13] Open Ephys Wiki, "Possible Projects and Future Development," <https://open-ephys.atlassian.net/wiki/>, 2015.
- [14] A. Palumbo, F. Amato, B. Calabrese, M. Cannataro, G. Cocorullo, A. Gambardella, P. Guzzi, M. Lanuzza, M. Sturniolo, P. Veltri, and P. Vizza, "An Embedded System for EEG Acquisition and Processing for Brain Computer Interface Applications," *Wearable and Autonomous Biomedical Devices and Systems for Smart Environments*, vol. 75, 2015.
- [15] J. Mercado, J. Herrera, A. de Jesus Plansza, and J. Guitierrez, "Embedded EEG Recording Module with Active Electrodes for Motor Imagery Brain-Computer Interface," *IEEE Latin America Transactions*, vol. 75, 2016.
- [16] M. Aravind and S. Babu, "Embedded Implementation of Brain Computer Interface Concept Using FPGA," *International Journal of Science and Research*, 2015.
- [17] I. Ozden, M. Sullivan, M. Lee, and S. Wang, "Reliable Coding Emerges from Coactivation of Climbing Fibers in Microbands of Cerebellar Purkinje Neurons," *Journal of Neuroscience*, vol. 29, no. 34, 2009.
- [18] V. Gauck and D. Jaeger, "The Control of Rate and Timing of Spikes in the Deep Cerebellar Nuclei by Inhibition," *Journal of Neuroscience*, vol. 20, no. 8, 2000.
- [19] M. Sullivan, A. Nimmerjahn, D. Sarkisov, F. Helmchen, and S.-H. Wang, "In Vivo Calcium Imaging of Circuit Activity in Cerebellar Cortex," *Journal of Neurophysiology*, vol. 94, 2005.
- [20] P. Yarmolenko, E. J. Moon, C. Landon, A. Manzoor, D. Hochman, B. Viglianti, and M. Dewhirst, "Thresholds for Thermal Damage to Normal Tissue: An Update," *International Journal of Hyperthermia*, 2013.
- [21] N. Matsumi, K. Matsumoto, N. Mishima, E. Moriyama, T. Furuta, A. Nishimoto, and K. Taguchi, "Thermal Damage Threshold of Brain Tissue – Histological Study of Heated Normal Monkey Brains," *Neurol Med Chir*, 1993.
- [22] P. Wolf, "Thermal Considerations for the Design of an Implanted Cortical Brain-Machine Interface (BMI)," *Indwelling Neural Implants: Strategies for Contending with the In Vivo Environment*, 2008.
- [23] P. Kohler, C. Linsmeier, J. Thelin, M. Bengtsson, H. Jorntell, M. Garwicz, J. Schouenborg, and L. Wallman, "Flexible Multi-Electrode Brain-Machine Interface for Recording in the Cerebellum," *IEEE Engineering Medicine Biology Society*, vol. 536, no. 8, 2009.
- [24] S. Kaxiras and M. Martonosi, "Computer Architecture Techniques for Power Efficiency," *Synthesis Lecture Series*, 2009.
- [25] C. Lefurgy, K. Rajamani, F. Rawson, W. Felter, M. Kistler, and T. Keller, "Energy Management for Commercial Servers," *IEEE Computer*, vol. 36, no. 12, 2003.
- [26] S. Herbert and D. Marculescu, "Analysis of Dynamic Voltage/Frequency Scaling in Chip Multiprocessors," *International Symposium on Low Power Electronics and Design*, 2007.
- [27] Q. Deng, D. Meisner, A. Bhattacharjee, T. Wenisch, and R. Bianchini, "MultiScale: Memory System DVFS with Multiple Memory Controllers," *International Symposium on Low Power Electronics and Design*, 2012.
- [28] Q. Deng, D. Meisner, A. Bhattacharjee, T. Wenisch, and R. Bianchini, "CoScale: Coordinating CPU and Memory System DVFS in Server Systems," *International Symposium on Microarchitecture*, 2012.
- [29] Q. Deng, D. Meisner, L. Ramos, T. Wenisch, and R. Bianchini, "MemScale: Active Low-Power Modes for Main Memory," *International Conference on Architectural Support for Programming Languages and Operating Systems*, 2011.
- [30] A. Bhattacharjee and M. Martonosi, "Thread Criticality Predictors for Dynamic Performance, Power, and Resource Management in Chip Multiprocessors," *International Symposium on Computer Architecture*, 2009.
- [31] J. Li, J. Martinez, and M. Huang, "The Thrifty Barrier: Energy-Aware Synchronization in Shared-Memory Multiprocessors," *International Symposium on High Performance Computer Architecture*, 2004.
- [32] D. Meisner and T. Wenisch, "DreamWeaver: Architectural Support for Deep Sleep," *International Conference on Architectural Support for Programming Languages and Operating Systems*, 2012.
- [33] D. Meisner, C. Sadler, L. Barroso, W.-D. Webber, and T. Wenisch, "Power Management of On-Line Data Intensive Services," *International Symposium on Computer Architecture*, 2011.
- [34] D. Meisner, B. Gold, and T. Wenisch, "PowerNap: Eliminating Server Idle Power," *International Conference on Architectural Support for Programming Languages and Operating Systems*, 2009.
- [35] D. Jimenez and C. Lin, "Dynamic Branch Prediction with Perceptrons," *International Symposium on High Performance Computer Architecture*, 2001.
- [36] D. Jimenez, "Fast Path-Based Neural Branch Prediction," *International Symposium on Computer Architecture*, 2003.
- [37] D. Jimenez, "Piecewise Linear Branch Prediction," *International Symposium on Computer Architecture*, 2005.
- [38] R. S. Amant, D. Jimenez, and D. Burger, "Low-Power, High-Performance Analog Neural Branch Prediction," *International Symposium on Microarchitecture*, 2008.
- [39] D. Jimenez and C. Lin, "Neural Methods for Dynamic Branch Prediction," *ACM Transactions on Architecture and Code Optimization*, 2002.
- [40] J. Lee and J. Smith, "Branch Prediction Strategies and Branch Target Buffer Design," *IEEE Computer*, vol. 17, no. 1, 1985.
- [41] J. Smith, "A Study of Branch Prediction Strategies," *International Symposium on Computer Architecture*, 1981.
- [42] S. McFarling, "Combining Branch Predictors," *Technical Report*

- TN-36m, Digital Western Lab, 1993.
- [43] T.-Y. Yeh and Y. Patt, "Two-Level Adaptive Training Branch Prediction," *International Symposium on Microarchitecture*, 1991.
- [44] A. Sez nec, "Analysis of the O-GEometric History Length Branch Predictor," *International Symposium on Computer Architecture*, 2005.
- [45] A. Sez nec, "The L-TAGE Predictor," *Journal of Instruction Level Parallelism*, 2007.
- [46] A. Sez nec, "An Optimized Scaled Neural Branch Predictor," *International Conference on Computer Design*, 2011.
- [47] "Human Cerebellum Image," *Life Science Databases/Wikimedia Commons*.
- [48] B. Barbour, "Equipe Cervelet," <http://www.ibens.ens.fr>.
- [49] D. Tank, M. Sugimori, J. Connor, and R. Llinas, "Spatially Resolved Calcium Dynamics of Mammalian Purkinje Cells in Cerebellar Slice," *Science*, vol. 242, 1998.
- [50] M. Bielawski and H. Bondurant, "Psychosis Following a Stroke to the Cerebellum and Midbrain: A Case Report," *Cerebellum and Ataxias*, 2015.
- [51] H. Picard, I. Amado, S. Mouchet-Mages, J.-P. Olie, and M.-O. Krebs, "The Role of the Cerebellum in Schizophrenia: An Update of Clinical, Cognitive, and Functional Evidences," *Schizophrenia Bulletin*, vol. 34, no. 1, 2008.
- [52] G. Kaloshi, V. Alikaj, A. Rroji, G. Vreto, and M. Petrela, "Visual and Auditory Hallucinations Revealing Cerebellar Extraventricular Neurocytoma: Uncommon Presentation for Uncommon Tumor in Uncommon Location," *General Hospital Psychiatry*, vol. 35, no. 6, 2013.
- [53] "Utah array," <http://churchlandlab.neuroscience.columbia.edu/images/utahArray.jpg>.
- [54] "Utah array plugged into brain tissue," <http://prometheus.med.utah.edu/bwjones/wp-content/uploads/iblog/Implant1.jpg>.
- [55] R. Kelly, M. Smith, J. Samonds, A. Kohn, A. Bonds, J. Movshon, and T. Lee, "Comparison of Recordings from Microelectrode Arrays and Single Electrodes in the Visual Cortex," *Journal of Neuroscience*, vol. 27, no. 2, 2007.
- [56] S. Suner, M. Fellows, C. Vargas-Irwin, G. Nakata, and J. Donoghue, "Reliability of Signals From a Chronically Implanted, Silicon-Based Electrode Array in Non-Human Primate Primary Motor Cortex," *IEEE Transactions on Neural Systems and Rehabilitation Engineering*, 2005.
- [57] C. Nordhausen, E. Maynard, and R. Normann, "Single Unit Recording Capabilities of a 100 Microelectrode Array," *Brain Res*, 1996.
- [58] S. Cooreman, "Power-Saving Tips When Rapid Prototyping ARM Cortex-M MCUs," <http://electronicdesign.com/power/power-saving-tips-when-rapid-prototyping-arm-cortex-m-mcus>, 2016.
- [59] C. D. Zeeuw, J. Simpson, C. Hoogenraad, N. Galjart, S. Koekkoek, and T. Ruigrok, "Microcircuitry and the Function of the Inferior Olive," *Trends in Neuroscience*, vol. 21, no. 9, 1998.
- [60] ST Microelectronics, "Ultra-low-power ARM Cortex-M4 32-bit datasheet," <http://www.st.com/content/ccc/resource/technical/document/datasheet/>, 2016.
- [61] K. Y. Kwon, S. Eldawaty, and K. Oweiss, "NeuroQuest: A Comprehensive Analysis Tool for Extracellular Neural Ensemble Recording," *Journal of Neuroscience Methods*, vol. 204, no. 1, 2012.
- [62] A. Baniyadi and A. Moshovos, "Branch Predictor Prediction: A Power-Aware Branch Predictor for High-Performance Processors," *ICCD*, 2002.
- [63] D. Parikh, K. Skadron, Y. Zhang, M. Barcella, and M. Stan, "Power Issues Related to Branch Prediction," *HPCA*, 2002.
- [64] N. Muralimanohar, R. Balasubramonian, and N. Jouppi, "CACTI 6.0: A Tool to Model Large Caches," *International Symposium on Microarchitecture*, 2007.
- [65] S. Li, J. H. Ahn, R. Strong, J. Brockman, D. Tullsen, and N. Jouppi, "McPAT: An Integrated Power, Area, and Timing Modeling Framework for Multicore and Manycore Architectures," *International Symposium on Microarchitecture*, 2009.
- [66] E. Teran, Z. Wang, and D. Jimenez, "Perceptron Learning for Reuse Prediction," *International Symposium on Microarchitecture*, 2016.
- [67] H. Sharma, J. Park, D. Mahajan, E. Amaro, J. K. Kim, C. Shao, A. Mishra, and H. Esmailzadeh, "From High-Level Deep Neural Models to FPGAs," *International Symposium on Microarchitecture*, 2016.
- [68] Y.-H. Chen, T. Krishna, J. Emer, and V. Sze, "14.5 Eyeriss: An Energy-Efficient Reconfigurable Accelerator for Deep Convolutional Neural Networks," *International Solid State Circuits Conference*, 2016.
- [69] A. Joshi, V. Yousofzadeh, V. Vemana, T. McGinnity, G. Prasad, and K. Wong-Lin, "An Integrated Modelling Framework for Neural Circuits with Multiple Neuromodulators," *Journal of the Royal Society Interface*, 2017.
- [70] Y. Sen, M. Ferdman, and P. Milner, "Maximizing CNN Accelerator Efficiency Through Resource Partitioning," *International Symposium on Computer Architecture*, 2017.
- [71] M. Alwani, H. Chen, M. Ferdman, and P. Milner, "Fused-Layer CNN Accelerators," *International Symposium on Microarchitecture*, 2016.
- [72]
- [73] Y. Chen, T. Luo, S. Liu, S. Zhang, L. He, J. Wang, L. Li, T. Chen, Z. Xu, N. Sun, and O. Temam, "DaDianNao: A Machine-Learning Supercomputer," *International Symposium on Microarchitecture*, 2014.
- [74] T. Chen, Z. Du, N. Sun, J. Wang, C. Wu, Y. Chen, and O. Temam, "A Small-Footprint High-Throughput Accelerator for Ubiquitous Machine Learning," *International Conference on Architectural Support for Programming Languages and Operating Systems*, 2004.
- [75] A. Hashmi, H. Berry, O. Temam, and M. Lipasti, "Automatic Abstraction and Fault Tolerance in Cortical Microarchitectures," *International Symposium on Computer Architecture*, 2008.
- [76] A. Nere, A. Hashmi, M. Lipasti, and G. Tononi, "Bridging the Semantic Gap: Emulating Biological Neuronal Behavior with Simple Digital Neurons," *International Symposium on High Performance Computer Architecture*, 2013.
- [77] J. Smith, "Efficient Digital Neurons for Large Scale Cortical Architectures," *International Symposium on Computer Architecture*, 2014.